nature photonics

Article

https://doi.org/10.1038/s41566-023-01248-3

Spin-selective strong light–matter coupling in a 2D hole gas-microcavity system

Received: 1 February 2023

Accepted: 26 May 2023

Published online: 03 July 2023

Check for updates

D. G. Suárez-Forero [1] ✉, D. W. Session[1], M. Jalali Mehrabad [1], P. Knüppel [2], S. Faelt[3,4], W. Wegscheider [3] & M. Hafezi [1,5] ✉

The interplay between time-reversal symmetry breaking and strong light–matter coupling in two-dimensional (2D) gases brings intriguing aspects to polariton physics. This combination can lead to a polarization/spin-selective light–matter interaction in the strong coupling regime. Here we report such a selective strong light–matter interaction by harnessing a 2D gas in the quantum Hall regime coupled to a microcavity. Specifically, we demonstrate circular-polarization dependence of the vacuum Rabi splitting, as a function of magnetic field and hole density. We provide a quantitative understanding of the phenomenon by modelling the coupling of optical transitions between Landau levels to the microcavity. This method introduces a control tool over the spin degree of freedom in polaritonic semiconductor systems, paving the way for new experimental possibilities in light–matter hybrids.

A gas of charged particles confined in two dimensions has been a cornerstone system to investigate numerous single-particle and many-body quantum-mechanical effects. In these systems, the reduction in dimensionality has enabled the demonstration of integer[1,2] and fractional[3] quantum Hall effects, Mott-insulating phases[4,5], superconductivity[6], the formation of skyrmions[7,8] and spin-ordered states[9], among other effects[10]. Recently, the possibility of coupling such two-dimensional (2D) gases to an optical mode, forming cavity exciton-polaritons, has opened up exciting new prospects. For example, this capability has been exploited to optically study integer and fractional quantum Hall states[11,12], the formation of skyrmions and manipulation of the magnetic Landé *g*-factor[13], and the enhancement of optical nonlinearities, when an electron gas, in the fractional quantum Hall regime, is dressed with the cavity mode[14]. Recent experiments have also demonstrated giant Zeeman splitting and valley-selective light–matter coupling in a monolayer transition-metal dichalcogenide (TMD)[15]. The demonstration of the mentioned effects requires that the light–matter interaction strength in the microcavity exciton-polaritons exceeds cavity and matter dissipation—a regime known as strong coupling (SC)[16].

Combining SC with broken time-reversal symmetry in chiral systems is expected to unlock new perspectives for the optical manipulation of correlated states of matter[17–19]. The chirality can arise from either electronic or photonic degrees of freedom, and in the exciton-polariton systems, these two are intertwined. The work decribed in this Article illustrates a method to induce a strong spin-selectivity in the light–matter coupling between an electronic transition and a cavity mode. To achieve this, we use a hole (h^+) gas in a semiconductor quantum well (QW), embedded in a microcavity. The system is subjected to an external magnetic field (B) so as to be in the quantum Hall regime. The modification of the density of states induced by B results in the selectivity of the light–matter coupling for each circularly polarized state of light. We explain this selectivity, in a single-particle picture, by combining an exciton-polariton model and the Landau-level filling picture. We note that the robustness of this mechanism is demonstrated at a temperature of 3.5 K, where the Coulomb-induced matter correlations are expected to be irrelevant.

Results

System description

Our physical system consists of a doped GaAs QW whose electronic states can be manipulated either through an applied gate voltage or a magnetic field. The sample is a p-doped grown QW, which constitutes a 2D h^+ gas (2DHG). To strongly enhance the interaction with an electromagnetic mode, the QW is embedded in a distributed Bragg reflector (DBR) semiconductor microcavity. Such a hybrid system provides a powerful tool to analyse electron spin properties via optical

[1]Joint Quantum Institute, University of Maryland, College Park, MD, USA. [2]Laboratory of Atomic and Solid State Physics, Cornell University, Ithaca, NY, USA. [3]Solid State Physics Laboratory, ETH Zürich, Zurich, Switzerland. [4]Institute of Quantum Electronics, ETH Zürich, Zurich, Switzerland. [5]Pauli Center for Theoretical Studies, ETH Zürich, Zurich, Switzerland. ✉e-mail: dsuarezf@umd.edu; hafezi@umd.edu

https://doi.org/10.1038/s41566-023-01248-3

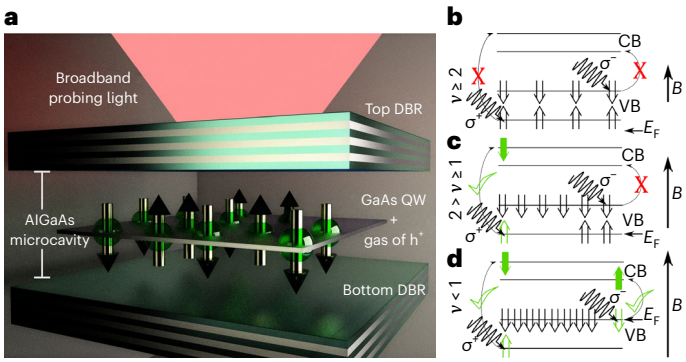

Fig. 1 | System description and physical mechanisms. a, Diagram of the sample, including an illustration of the 2DHG embedded in an optical microcavity. **b**–**d**, Mechanism to induce spin-selectivity for light–matter coupling, benchmarked by three ranges of the filling factor ν. VB, valence band; CB, conduction band. **b**, For $\nu \geq 2$, none of the spin VBs has available states and therefore no electronic transition can take place. As a consequence, the SC regime will not be reached. **c**, As the magnetic field increases and enters the $1 \leq \nu < 2$ regime, the density of states is tuned such that the σ^+ subband becomes available. Unlike the former case, the electronic transition is not blocked anymore, and this spin population reaches the SC regime. The σ^- states are still Pauli-blocked, so no electronic transition is allowed for them. The result is spin-selective light–matter coupling. **d**, As B is further increased such that the system is tuned into the $\nu < 1$ regime, the σ^- band starts to have available states and can reach SC. The asymmetry in the Rabi frequency persists because the σ^- band is still populated, in contrast to the σ^+ band, which is fully available. The Fermi energy (E_F) is indicated for each regime in **b**–**d**.

experiments by exploiting the selection rules that determine a spin-selective transition depending on the circular polarization of light. The origin of this selectivity is in the crystalline structure and spin–orbit coupling properties of GaAs QWs, whose upper valence band is a heavy hole band (with total angular momentum $J_z^h = \pm 3/2$). A schematic representation of the 2D gas of semi-integer spin-charged particles confined to the QW and interacting with the electromagnetic field is presented in Fig. 1a. All data shown in the main text are obtained at 3.5 K, where we do not expect any correlated electron physics to be present. A more detailed discussion of the selection rules and comparison to 40-mK data are provided in Supplementary Sections 1 and 3, respectively. Details of the sample composition and fabrication can be found in Methods.

Mechanism for spin-selective SC

An external magnetic field acting on the 2D gas induces Landau levels that are non-degenerate for the spin eigenstates. This spin energy splitting depends on the magnitude of B and, in particular for a h^+ doped system, it has a strong dependence on the particle density due to the spin–orbit interaction [20,21]. At the same time, the h^+ density and the magnetic field determine the Fermi energy and hence the existence of an optically active transition of the electrons in the valence band[22,23]. We exploit this particular interplay to obtain a spin-selective light–matter interaction. Specifically, for a fixed density of particles, we tune B to consider three relevant situations with fundamentally different light–matter coupling properties. The quantity that determines the three cases is the quantum Hall filling factor $\nu = \rho/n_B$, defined as the ratio between the h^+ density ρ and the density of magnetic states $n_B = eB/h$ (e is the electron charge and h is Planck's constant). The three cases are depicted in Fig. 1b–d. The first scenario (Fig. 1b) takes place when $\nu \geq 2$. In this condition, there are no available states in any of the two spin subbands, inhibiting the possibility of an electronic transition from the lowest Landau level and therefore keeping the system in the so-called weak coupling regime. The next situation takes place when $1 \leq \nu < 2$ (Fig. 1c). In this case, one of the subbands (σ^-) is still full, but the opposite spin state (σ^+) can instead host optically generated electron–hole pairs, leading to a polarization-selective SC. Finally, when $\nu < 1$, as shown in Fig. 1d, both spin transitions are open, but, due to the imbalance in the h^+ population, the system still has strong asymmetry in the light–matter coupling.

Optical measurements

To investigate the proposed mechanism, we performed angular and spectrally resolved reflectivity measurements to reconstruct the energy dispersion in a confocal set-up. Such a set-up is capable of mapping the far-field for any polarization state, using a broadband light source for excitation. A complete description of the optical set-up is provided in Methods. Density ρ is manipulated via a gate voltage and is set to ~9.4×10^{10} cm^{-2}, a density high enough to guarantee that at low B, both spin valence subbands (σ^+ and σ^-) are occupied, but low enough to allow the desired effect to take place at a few teslas; that is, the higher the density, the higher the magnetic field at which the conditions $\nu = 2$ and $\nu = 1$ take place. We sweep B to tune the system over a range of filling factors that covers the three regimes described in Fig. 1b–d. Figure 2 shows the measured dispersion of the exciton-polariton system for both circular polarizations and values of B in the three ranges of ν. For $\nu \geq 2$, as shown in Fig. 2a,b, and in agreement with the above description, only the parabolic dispersion from a bare cavity mode can be observed. This indicates that none of the spin subbands have available states and hence no optical electronic transition can take place. Next, by increasing B, we reach the $2 > \nu \geq 1$ regime, and the asymmetry in SC is then manifested. Although the dispersion is still parabolic for σ^- (Fig. 2c), the σ^+ channel has clearly reached the SC regime, as observed from the formation of lower and upper polariton branches in the energy dispersion (Fig. 2d). By further increasing B, we reach the regime $\nu < 1$ (Fig. 2e,f), where both spin subbands can now reach SC, but the asymmetry in the h^+ distribution causes the population of σ^- to couple less efficiently to the cavity mode than the population in the σ^+ subband. As a consequence, the vacuum Rabi splitting is different for each state of circular polarization.

A coupled oscillator model was used for the quantitative analysis of our observation, characterized by the polaritonic Hamiltonian:

$$\hat{H} = \sum_k \left(\omega_c + \frac{k^2}{2m}\right)\hat{a}_k^\dagger \hat{a}_k + \omega_X \sum_k \hat{b}_k^\dagger \hat{b}_k + \Omega \sum_k \left(\hat{b}_k^\dagger \hat{a}_k + \hat{b}_k \hat{a}_k^\dagger\right) \quad (1)$$

for each polarization, where ω_c is the cavity mode's energy, k its momentum, m its effective mass, and $\omega_X(B)$ and $\Omega(B)$ are the energy of the electronic transition and the Rabi splitting, respectively (the latter two quantities depend on B). The operators $\hat{a}_k$ correspond to the annihilation operators of the cavity mode k, and $\hat{b}_k$ to the electronic transition with corresponding momentum k (ref. 24). An example of the obtained polaritonic eigenfunction after fitting the data is included in Fig. 2f. The cavity and exciton modes are depicted (dotted red lines) together with the upper and lower polariton branches (dashed blue lines) that match the experimental dispersion.

The trend of spin-selective light–matter coupling as a function of the filling factor is illustrated in Fig. 3. To obtain this, we extract a vertical section of the energy dispersion corresponding to the momentum at which the bare cavity and electronic transition cross (deduced from the theoretical model). From Fig. 3 one can observe how the filling factor $\nu = 2$ benchmarks the establishment of SC for σ^+, which is observed as the emergence of two resonances instead of one, while σ^- remains decoupled. Only for filling factors above $\nu = 1$ can the two polariton resonances be observed for this spin state, although, as previously mentioned, there is a persistent difference in the value of Ω. Here it is worth noting the feeble trace of the opposite spin reflection contrast that can be detected on each panel of Fig. 3. We associate this with three effects: imperfections in the polarization

https://doi.org/10.1038/s41566-023-01248-3

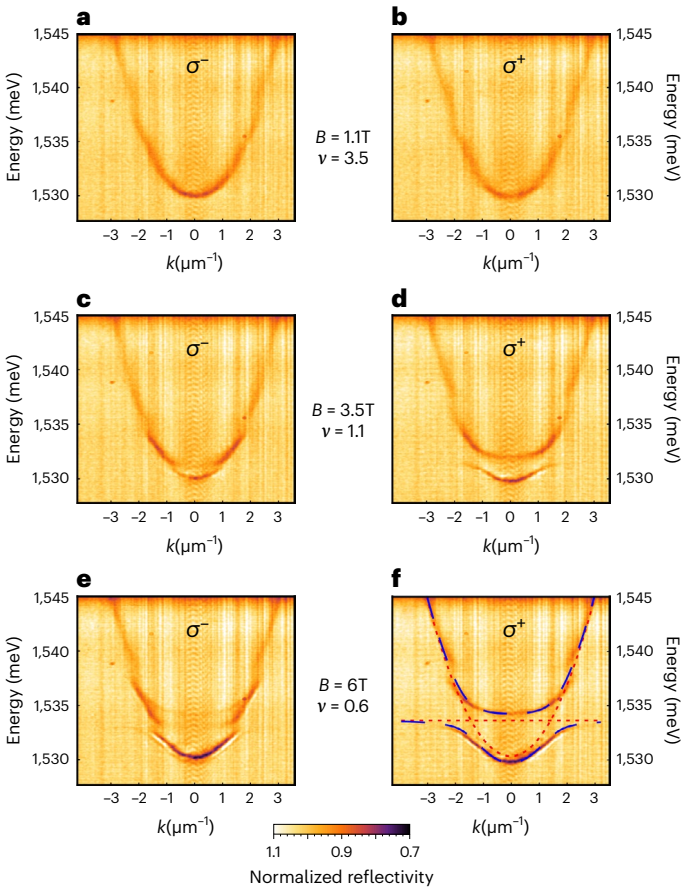

Fig. 2 | Energy dispersion of the system probed at values of *B* corresponding to the three ranges of *ν* shown in Fig. 1b–d. a–**f**, Energy dispersion of the system for σ^- polarization (**a**,**c**,**e**) and σ^+ polarization (**b**,**d**,**f**). **a**,**b**, When $\nu \geq 2$, both spin subbands are occupied and no electronic transition can take place in the system. Only the bare cavity mode is visible. **c**,**d**, In the regime $2 > \nu \geq 1$, only the σ^+ spin subband has available states, and hence spin-selectivity manifests. Only the dispersion probed with σ^+ polarization shows polaritonic bands, while σ^- remains decoupled. **e**,**f**, On further increasing *B*, the σ^- population can also reach SC, but the remaining h^+ population in this subband makes the light–matter coupling asymmetric, causing the Rabi splitting to be larger for σ^+. In **f**, the fitting obtained from a theoretical model (equation (1)) is also shown. Cavity and exciton modes are depicted as red dotted lines, and the upper and lower polariton branches are depicted as dashed blue lines.

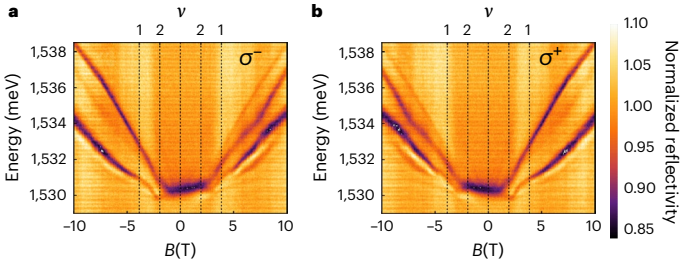

Fig. 3 | Magnetic field dependence of the system resonance at the momentum at which the bare cavity and exciton energies cross. a,**b**, Due to both Zeeman splitting and the diamagnetic shift, this crossing occurs at different momentums for each *B*. The values of *B* for filling factors 1 and 2 that delimit the three regimes of the system are indicated by black dotted lines for positive and negative values of *B*. Data are displayed for both spin states σ^- (**a**) and σ^+ (**b**).

filters, linear birefringence of the cavity and transverse-electric–transverse-magnetic splitting. The birefringence has the capability of changing the system's polarization, and the transverse-electric–transverse-magnetic splitting shows the capability of introducing intrinsic chiral behaviour in the system[25]. The evolution of the full energy dispersion with a magnetic field is shown in Supplementary Video 1.

To obtain a quantitative description of the spin-selective SC effect, we extracted the values of ω_X and Ω from the described theoretical model for each magnitude of *B* and for each spin state. The results are displayed in Fig. 4. From the Rabi splitting value (Fig. 4a–c), one can observe how the integer filling factors (marked on the top axis) coincide with the magnetic fields at which the populations σ^+ and σ^- reach the SC ($\nu = 2$ and $\nu = 1$, respectively). As previously mentioned, for $\nu < 1$, the asymmetry in Ω persists due to the h^+ population in the σ^- subband; we expect that, for even higher magnetic fields, the difference will be asymptotically eliminated as $\nu \to 0$. Notice that for $\nu < 1$, Ω further increases for the σ^+ polariton resonances. This is due to the electron and hole confinement induced by the magnetic field that increases the oscillator strength and hence Ω (ref. 26). Finally, for a fully depleted h^+ gas (Fig. 4c), the selectivity is completely removed, and both spin subbands are in SC with the cavity mode, in agreement with the expected behaviour of a polaritonic system. The Supplementary videos show the fitting of the energy dispersion with a variable magnetic field, for the densities studied in this Article.

Discussion

The theoretical model (equation (1)), in close agreement with experimental observations, provides the value of the electronic transition energy (Fig. 4d,e). However, it is important to mention that a complete understanding of the nature of this optically induced transition requires further experimental and theoretical investigations. Although the existence of the transition depends on the filling factor, its microscopic properties are determined by the interplay between (1) the electron–hole Coulomb interaction, (2) the interaction with the 2DHG and (3) the interaction with the external magnetic field. As none of these interactions dominates over the other two, a complete description of this polaritonic quasi-particle is not straightforward. Indeed, recent theoretical efforts have been directed to investigate the nature of the light–matter coupling under these circumstances[27]. It is also important to highlight that, although the nature of this quasi-particle remains the subject of active research, the demonstration of selective coupling to the cavity mode does not depend on it. Hence, the results presented in this Article remain valid, regardless of the nature of the matter excitation.

Asymmetry in the light–matter coupling has been reported for similar systems at lower charge densities when the 2DHG is in a spin-ordered state in the frame of integer or fractional quantum Hall effects[12,13,28]. In those cases, the asymmetry takes place for specific values of *B* at which correlated states of matter dominate. This is not the case for the system studied in this Article. In our case, any trace of correlated matter states at integer filling factors is ruled out by increasing the temperature (*T*) of the system to 3.5 K (in contrast to refs. 12,13, where *T* is kept at ~100 mK). The fact that the presented results are collected at a relatively high *T* (3.5 K) indicates that our observation is not related to many-body electronic correlations, highlighting the robustness of this mechanism. The Supplementary Information includes a comparison between the system's responses at 40 mK and 3.5 K (Supplementary Section 3) as well as the method for calibrating the h^+ density that requires these ultra-low values of *T* (Supplementary Section 2).

In summary, we have introduced an experimental method for spin-selective light–matter coupling in a microcavity-QW system by modification of the hole density and the strength of the applied magnetic field. This result opens up perspectives for the control

https://doi.org/10.1038/s41566-023-01248-3

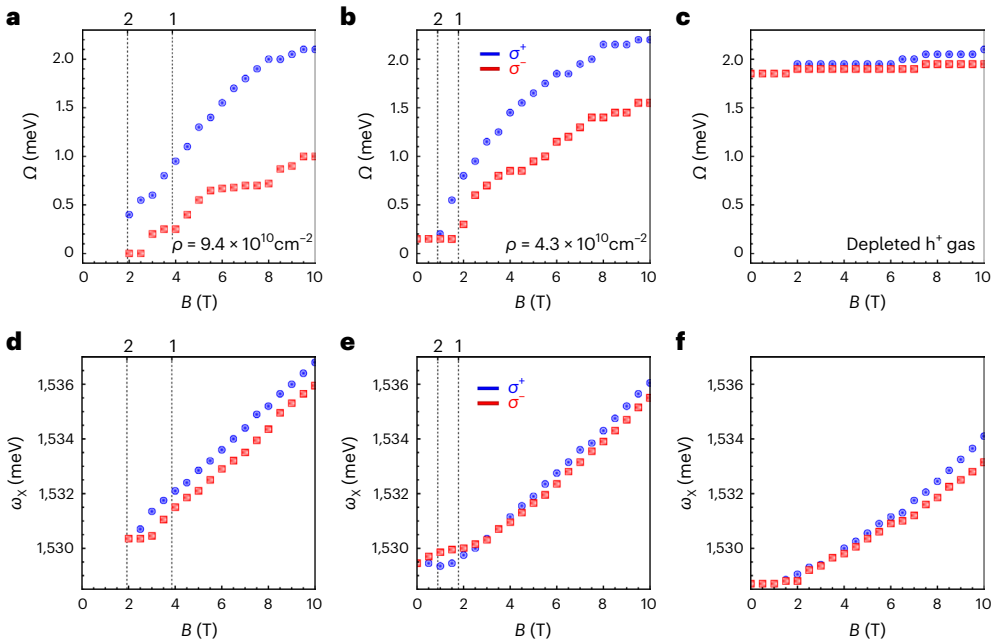

Fig. 4 | Quantitative description of the spin-selective SC effect. a–c, Rabi splitting obtained from fitting to a polariton model (equation (1)) for selected magnetic fields and for three different h^+ densities. **d–f**, Energy of the electronic transition obtained from the theoretical model for the same selected magnetic fields and densities. **a**,**d**, $\rho = 9.4 \times 10^{10}$ cm^{-2}. **b**,**e**, $\rho = 4.3 \times 10^{10}$ cm^{-2}. **c**,**f**, Fully depleted h^+ gas. As expected, light–matter coupling selectivity is not observed in **c**,**f**.

of nonlinear effects in light–matter hybrid systems. For example, in exciton-polariton systems, the $\chi^{(3)}$ optical nonlinearity could be easily controlled using the polarization of the light. As shown in Supplementary Fig. 4, the spin-selectivity persists even at lower temperatures (~40 mK), where correlated states of electrons are expected, such as fractional quantum Hall states. However, samples with higher mobilities are required to further investigate the interplay between spin selection and correlated states of electrons.

Importantly, applications of this method are not limited to III–V semiconductor devices. One potential alternative platform comprises the transition-metal dichalcogenide materials, in which spin and valley degrees of freedom are locked. The present method, combined with the possibility of embedding a monoatomic semiconductor in a 2D microcavity[29], suggests interesting potential for the valley-selective light–matter SC previously reported in the literature[15]. This versatility is also expected to unlock the experimental realization of recent theoretical proposals for the optical study and manipulation of the light–matter interaction in different 2D correlated matter systems. Although this perspective is very promising, a deep theoretical understanding of these phenomena is still under development[30–32]. Overcoming both the technical and conceptual challenges promises to pave the way for the investigation of this exotic physics. Our system might also enable technological implementations such as variable circular polarization filters with ultra-narrow bandwidth, and, from a more fundamental point of view, it is a suitable platform to optically study the spin physics of 2D gases of charged fermions, thanks to the degree of control of the light–matter interaction that can be achieved by modifying the h^+ density.

Online content

Any methods, additional references, Nature Portfolio reporting summaries, source data, extended data, supplementary information, acknowledgements, peer review information; details of author contributions and competing interests; and statements of data and code availability are available at https://doi.org/10.1038/s41566-023-01248-3.

References

1. VonKlitzing, K. The quantized Hall effect. *Rev. Mod. Phys.* **58**, 519–531 (1986).
2. Klitzing, K. V., Dorda, G. & Pepper, M. New method for high-accuracy determination of the fine-structure constant based on quantized Hall resistance. *Phys. Rev. Lett.* **45**, 494–497 (1980).
3. Stormer, H. L. Two-dimensional electron correlation in high magnetic fields. *Phys. B* **177**, 401–408 (1992).
4. Kawasugi, Y. et al. Two-dimensional ground-state mapping of a Mott-Hubbard system in a flexible field-effect device. *Sci. Adv.* **5**, eaav7282 (2019).
5. Li, T. et al. Continuous Mott transition in semiconductor moiré superlattices. *Nature* **597**, 350–354 (2021).
6. Cao, Y. et al. Unconventional superconductivity in magic-angle graphene superlattices. *Nature* **556**, 43–50 (2018).
7. Schmeller, A., Eisenstein, J. P., Pfeiffer, L. N. & West, K. W. Evidence for skyrmions and single spin flips in the integer quantized Hall effect. *Phys. Rev. Lett.* **75**, 4290–4293 (1995).
8. Shukla, S., Shayegan, M., Parihar, S., Lyon, S. & Cooper, N. Large skyrmions in an $Al_{0.13}Ga_{0.87}As$ quantum well. *Phys. Rev. B* **61**, 4469–4472 (2000).
9. Zuo, Z.-W. et al. Quantum Hall ferromagnets. *Rep. Prog. Phys.* **72**, 086502 (2009).
10. Bao, C., Tang, P., Sun, D. & Zhou, S. Light-induced emergent phenomena in 2D materials and topological materials. *Nat. Rev. Phys.* **4**, 33–48 (2021).
11. Smolka, S. et al. Cavity quantum electrodynamics with many-body states of a two-dimensional electron gas. *Science* **346**, 332–335 (2014).
12. Ravets, S. et al. Polaron polaritons in the integer and fractional quantum Hall regimes. *Phys. Rev. Lett.* **120**, 057401 (2018).
13. Lupatini, M. et al. Spin reversal of a quantum Hall ferromagnet at a Landau level crossing. *Phys. Rev. Lett.* **125**, 067404 (2020).
14. Knüppel, P. et al. Nonlinear optics in the fractional quantum Hall regime. *Nature* **572**, 91–94 (2019).

15. Lyons, T. P. et al. Giant effective Zeeman splitting in a monolayer semiconductor realized by spin-selective strong light–matter coupling. *Nat. Photon.* **16**, 632–636 (2022).
16. Carusotto, I. & Ciuti, C. Quantum fluids of light. *Rev. Mod. Phys.* **85**, 299–366 (2013).
17. Whittaker, C. E. et al. Optical analogue of Dresselhaus spin–orbit interaction in photonic graphene. *Nat. Photon.* **15**, 193–196 (2020).
18. Bloch, J., Cavalleri, A., Galitski, V., Hafezi, M. & Rubio, A. Strongly correlated electron-photon systems. *Nature* **606**, 41–48 (2022).
19. Hübener, H. et al. Engineering quantum materials with chiral optical cavities. *Nat. Mater.* **20**, 438–442 (2021).
20. Winkler, R. *Spin–Orbit Coupling Effects in Two-Dimensional Electron and Hole Systems*, Vol. 191 Springer Tracts in Modern Physics (Springer, 2003).
21. Ma, M. K. et al. Robust quantum Hall ferromagnetism near a gate-tuned $\nu = 1$ Landau level crossing. *Phys. Rev. Lett.* **129**, 196801 (2022).
22. Efimkin, D. K. & Macdonald, A. H. Exciton-polarons in doped semiconductors in a strong magnetic field. *Phys. Rev. B* **97**, 235432 (2018).
23. Rana, F., Koksal, O. & Manolatou, C. Many-body theory of the optical conductivity of excitons and trions in two-dimensional materials. *Phys. Rev. B* **102**, 85304 (2020).
24. Kavokin, A. V., Baumberg, J. J., Malpuech, G. & Laussy, F. P. *Microcavities* (Oxford Univ. Press, 2017).
25. Gianfrate, A. et al. Measurement of the quantum geometric tensor and of the anomalous Hall drift. *Nature* **578**, 381–385 (2020).
26. Cong, K., Noe, G. T. & Kono, J. Excitons in magnetic fields. *Encyclopedia Mod. Opt.* **1–5**, 63–81 (2018).
27. Laird, E., Marchetti, F. M., Efimkin, D. K., Parish, M. M. & Levinsen, J. Rydberg exciton-polaritons in a magnetic field. *Phys. Rev. B* **106**, 125407 (2022).
28. Chervy, T. et al. Accelerating polaritons with external electric and magnetic fields. *Phys. Rev. X* **10**, 011040 (2020).
29. Liu, X. et al. Strong light–matter coupling in two-dimensional atomic crystals. *Nat. Photon.* **9**, 30–34 (2015).
30. Graß, T. et al. Optical control over bulk excitations in fractional quantum Hall systems. *Phys. Rev. B* **98**, 155124 (2018).
31. Graß, T., Cotlet, O., Imamoğlu, A. & Hafezi, M. Optical excitations in compressible and incompressible two-dimensional electron liquids. *Phys. Rev. B* **101**, 155127 (2020).
32. Cao, B., Grass, T., Solomon, G. & Hafezi, M. Optical flux pump in the quantum Hall regime. *Phys. Rev. B* **103**, L241301 (2021).

Methods

Sample fabrication and preparation

Our sample consisted of an $Al_{0.2}Ga_{0.8}As$ λ cavity embedded between two AlAs/$Al_{0.2}Ga_{0.8}As$ DBRs (24 bottom pairs and 19 top pairs) with a p-doping (carbon) layer and a 16-nm GaAs QW, grown by molecular beam epitaxy. To control the h^+ density, a 60-nm Si-doped n-type GaAs layer was grown between the GaAs substrate and the bottom DBR. This acted as a gate to control the density of the 2DHG. Contacts were fabricated using In for the n-type GaAs gate and $In_{0.96}Zn_{0.04}$ for the 2DHG. The device's h^+ density could then be controlled by applying a gate voltage.

Set-up for optical measurements

The sample was placed in a dilution refrigerator with the capability of reaching temperatures down to 40 mK. Although all the measurements presented in this Article were taken at a temperature of 3.5 K, we performed measurements at a base temperature of 40 mK to calibrate the h^+ density, using the optical signature of correlated states at integer filling factors. The comparison of the data taken at the base temperature and 3.5 K, as well as details of the density calibration procedure, are available in Supplementary Sections 3 and 2, respectively.

For the optical measurements, we used a confocal set-up in a reflectivity configuration with numerical aperture of 0.5. A tungsten lamp was used as a broadband light source, but consistent results were obtained using a supercontinuum white-light source. Polarization-resolved spectra were collected by placing a linear polarizer followed by a quarter-wave plate in the excitation path.

Data availability

All of the data that support the findings of this study are reported in the main text, supplementary information and supplementary videos. Source data are available from the corresponding authors on reasonable request.

Acknowledgements

We thank A. Imamoglu and S. Ravets for valuable discussions and enriching feedback on the paper. This work was supported by grants AFOSR FA9550-20-1-0223, FA9550-19-1-0399, ONR N00014-20-1-2325, NSF IMOD DMR-2019444 and ARL W911NF1920181, M. Martin and the Simons Foundation. P.K. acknowledges financial support from the Swiss National Science Foundation.

Author contributions

D.G.S.-F. and M.H. conceived and designed the experiments. S.F. and W.W. designed and fabricated the microcavity-QW sample. D.W.S. processed the sample to adapt it for the required measurements. D.G.S.-F. performed the experiments. D.G.S.-F., M.H., M.J.M. and P.K. analysed the data and interpreted the results. D.G.S.-F., M.J.M. and M.H. wrote the paper, with input from all authors.

Competing interests

The authors declare no competing interests.

Additional information

Supplementary information The online version contains supplementary material available at https://doi.org/10.1038/s41566-023-01248-3.

Correspondence and requests for materials should be addressed to D. G. Suárez-Forero or M. Hafezi.

Peer review information *Nature Photonics* thanks Guillaume Malpuech and the other, anonymous, reviewer(s) for their contribution to the peer review of this work.